The dynamics of surface rearrangements in Si adatom diffusion on the Si{100}(2×1) surface

Deepak Srivastava and Barbara J. Garrison
Department of Chemistry, 152 Davey Laboratory, The Pennsylvania State University, University Park, Pennsylvania 16802

(Received 30 April 1991; accepted 26 July 1991)

The Si adatom adsorption and diffusion on the fully relaxed Si{100}(2×1) surface is studied by a combination of molecular dynamics simulations with Tersoff's potential for the Si interactions, a simplified transition state theory of Voter and lattice gas simulations. Six local minima for adsorption are found on the surface and the activation energies between each are determined. The Arrhenius behavior for the macroscopic diffusion is found to be $D = 5.67\times10^{-3}\exp(-0.75\ \text{eV}/kT)\ \text{cm}^2/\text{s}$. In addition, it is found that the adatom diffusion is strongly anisotropic in nature and the direction of easy diffusion is perpendicular to the dimers (i.e., parallel to the dimer rows) of the original surface. The minimum energy path for the diffusion is found to be activated by the local unreconstruction (dimer opening) of the otherwise fully reconstructed surface.

I. INTRODUCTION

The molecular beam epitaxy (MBE) of Si on the Si{100}(2×1) surface provides a challenge for scientists to understand at the microscopic level.[1-8] In the experiments, atoms and molecules effuse from an oven source toward a substrate. The goal is usually to grow thin epitaxial films. The typical rate of deposition of these films is around one layer per minute.[1] Consequently, not only does the adsorption process have to be considered but one must account for diffusive events.[5-11] Understanding the microscopic origins of the Si adatom diffusion on the fully relaxed dimer reconstructed Si{100}(2×1) surface is particularly challenging because of the numerous adsorption sites and the possible correlation between the diffusion dynamics and the surface reconstruction.[9-11]

Aspects of the theoretical description of the MBE growth of Si on Si{100}(2×1) have been previously investigated.[4-8,12-15] We have shown that the initial adsorption occurs preferentially at the dangling bond site.[4,5] In addition we have identified mechanisms of dimer opening that lead to epitaxial growth and also interlayer diffusion.[4,5,8] Others have calculated the energy profile for an adatom on the surface.[12-15] In this study we combine the above approaches and add transition state theory[16] with lattice gas simulations to determine the overall diffusion processes. The combined approach of molecular dynamics (MD), simplified transition state theory (STST), and lattice gas (LG) calculations[17,18] is needed because of the dramatically different time scales for the adsorption and diffusion processes.

The combined MD-STST-LG approach exploits the strengths of each technique in addressing the MBE growth of Si on Si{100}(2×1). The initial stages of the growth such as the adsorption event are calculated explicitly with MD simulations. The next set of events in the real system is the diffusive motions of the adsorbed atoms. The time scale of these events is too long to be studied with direct MD simulations. A possible approach is to use TST with the same interaction potential as used in the MD simulations to calculate the rate constants. Recently Voter and Doll[17,18] have shown that omitting modifications such as the dynamic correction factor from TST yields rate constants within a few percent of the corrected values. We feel then that the simplified version of TST is the most appropriate for examining the diffusion on Si for several reasons. First, the system is strongly interacting with adsorption energies of 2–3.5 eV. Thus there will probably not be multiple hops between sites. Second, there is the possibility of several adsorption sites each with two to four different directions of escape. The initial goal is to examine anisotropies in the diffusion and orders of magnitude differences in the escape rates. In addition, it is not clear that the approximations in the empirical potentials are not more severe than the simplifications in the TST. Finally we use lattice gas simulations with the rate constants from STST to examine the anisotropies in the diffusive motion on a macroscopic scale.

Our calculations show that the diffusion coefficient follows the Arrhenius behavior with $D = 5.67\times10^{-3}\times\exp(-0.75\ \text{eV}/kT)\ \text{cm}^2/\text{s}$. The diffusion is strongly anisotropic in nature and the direction of easy diffusion is parallel to the dimer rows of the original surface. Both the quantitative values and the direction of anisotropy are in excellent agreement with recent scanning tunneling microscopy results.[19,20] Our calculations reveal that the diffusion is activated by the local unreconstruction (dimer opening) of the otherwise fully reconstructed surface and that it proceeds by the adatom jumping between the neighboring dimer bridge sites [labeled D in Fig. 1(a)] via the H sites on the same dimer row in the $[1\bar{1}0]$ direction.

In Sec. II we discuss the theoretical approach to single adatom diffusion on the strongly interacting fully relaxed substrate. Section III contains the application to the adsorption and diffusion dynamics of a Si adatom on the Si{100}(2×1) surface; we describe the main results of this work, and compare our results with recent experimental and theoretical investigations.

 0021-9606/91/216885-07$03.00

II. STST FOR STRONGLY INTERACTING SYSTEMS

In this section we outline the procedure for applying STST to the diffusion of a Si adatom on the fully relaxed Si{100}(2×1) surface. The basic ideas are the same as those proposed by Voter for doing classically exact adatom and cluster diffusion on metal surfaces.[18] The emphasis in this work is on the application to semiconductor systems, where due to surface reconstructions each unit cell may have several binding sites. In addition, locating transition state surfaces among these sites is not always straightforward.

In the STST approach the diffusion of an adatom is composed of random uncorrelated hops between neighboring binding sites. It is also assumed that the time taken between hops is generally much longer than the time required to complete a hop. This approximation is certainly valid since the interactions in the Si system are quite strong. Thus the total escape rate from a local binding site A is

$$k_A^{\mathrm{STST}} = \sum_{i=1,4} \nu_{Ai} \exp\left(\frac{-E_{Ai}}{kT}\right), \tag{1}$$

where the sum over i corresponds to the four escape directions from site A, E_{Ai} is the activation energy at 0 K for the jump in the direction i, and ν_{Ai} is the vibrational frequency for the jump Ai, as given by

$$\nu_{Ai} = \frac{\Pi_{j=1,3}\nu_A^j}{\Pi_{k=1,2}\nu_i^k}. \tag{2}$$

Here ν_A^j and ν_i^k are the real vibrational frequencies when the adatom is at the local minimum A and at the saddle point i, respectively. These quantities are evaluated from the positive eigenvalues of the (3×3) force constant matrices. In Eq. (1) it is assumed that the adatom in a local binding site can escape only along two orthogonal directions. If this assumption is not made then the summation in Eq. (1) must be replaced by an integral. The validity of this assumption is discussed below.

The activation energies E_{Ai} and the vibrational frequencies ν_{Ai} for use in Eqs. (1) and (2) are computed in the following manner. The adatom is constrained in a fixed lateral position on the surface. The adatom is aimed at the surface with a velocity corresponding to 0.026 eV. Using molecular dynamics the vertical position of the incoming adatom and all coordinates of the atoms in the top few layers of the substrate are allowed to relax for about 1.5 ps (1 ps = 10^{-12} s). The entire system is then cooled slowly (3–5 ps) during which each velocity component of all atoms is independently set to zero as it passes through a maximum value. As the entire system is cooled to near 0 K the total energy of the system is minimized and simultaneously the normal force on the adatom is zero. We note that the relaxation time (1.5 ps) should be chosen sufficiently long such that the energy generated in the exothermic adatom/surface reaction is completely dissipated.[5,8] This procedure is repeated for a grid of lateral positions within a unit cell on the surface. In the case of Si{100}(2×1) the initial grid spacing was 0.24 Å. The search for stationary points corresponding to all the binding sites and the transition states is performed by a two-dimensional Newton–Raphson root finding method. For refinement of the minima and transition state energies and frequencies a grid spacing as small as 0.04 Å was used. Of note is that this cooling procedure brings the system to be at 0 K, thus the only temperature dependence in Eq. (1) is explicitly in the Boltzmann factor.

In any real system the activation energies and vibrational frequencies will also be modified by the temperature of the system. To include the effects of the thermal vibrations we modify the STST escape rates as

$$K_A = \sum_{i=1,4} K_{Ai}, \tag{3a}$$

with

$$K_{Ai} = k_{Ai}(1 + \Delta k_{Ai}/k_{Ai}). \tag{3b}$$

Here Δk_{Ai}, the first-order correction to the 0 K jump frequency k_{Ai}, is written as

$$\frac{\Delta k_{Ai}}{k_{Ai}} = \frac{\Delta \nu_{Ai}}{\nu_{Ai}} - \frac{\Delta E_{Ai}}{kT}. \tag{3c}$$

The change in the activation energy is given by

$$\Delta E_{Ai} = \Delta E_i - \Delta E_A, \tag{4a}$$

with

$$\Delta E_A = \langle E_A \rangle_T - E_A, \tag{4b}$$

and a similar expression for ΔE_i. Here $\langle E_A \rangle_T$ is the thermally averaged total energy of the system at temperature T when the adatom is constrained laterally at the 0 K position of site A. This thermal average is computed by performing MD calculations at a fixed temperature and calculating the thermal average of the total energy. In the calculations used below we used five independent trajectories of 3000 steps at each temperature. An analogous procedure for estimating the corrections to the vibrational frequencies would involve calculating the temperature-dependent position or velocity autocorrelation functions of the vibrating adatom. The convergence of these in time is generally slow and computationally intensive. Thus Eq. (2) can be rewritten as

$$\nu_{Ai} = \prod_{j \neq i} \left(\frac{\nu_A^j}{\nu_i^j}\right) \nu_A^i, \tag{5}$$

where the product $j \neq i$ includes all the vibrational frequencies except the frequency of the vibration ν_A^i along the direction $A \rightarrow i$. The temperature dependence in ν_{Ai} is then mainly through the temperature dependence of the one-dimensional harmonic vibrational frequency ν_A^i, which can be approximated by $\nu_A^i(T) = kT/\hbar$.[6] The thermal correction $\Delta\nu_{Ai}$ is then written as

$$\Delta\nu_{Ai}/\nu_{Ai} = [\nu_{Ai}(T)/\nu_{Ai} - 1], \tag{6}$$

where $\nu_{Ai}(T)$ is directly proportional to T and the expression in Eq. (6) can be written as

$$\Delta\nu_{Ai}/\nu_{Ai} = (T/T_{Ai}^0 - 1). \tag{7}$$

The reference temperature T_{Ai}^0 is fixed by knowing that as $T \rightarrow 0$, $\nu_{Ai}(T) \rightarrow \nu_{Ai}$ and $\Delta\nu_{Ai} \rightarrow 0$. We can invert Eq. (7) to write

$$T_{Ai}^0 = (1 + \Delta\nu_{Ai}/\nu_{Ai})^{-1} T, \tag{8}$$

and evaluate or approximate $\Delta\nu_{Ai} = \nu_{Ai}(T) - \nu_{Ai}$ at one low temperature. The temperature-dependent corrections to

the vibrational frequency at all higher temperatures are then estimated from Eq. (7). In our case we have assumed that the reference temperature for a jump $A \rightarrow i$ is 300 K and is the same for all possible jumps within the unit cell.

The last step in the calculation is to use the jump frequencies in a lattice gas simulation to compute the long range and long time scale diffusion. The idea behind the lattice gas calculations is that the adatom always resides in one or another local binding site. The diffusion of the adatom proceeds by randomly oriented hops between the neighboring binding sites with the probability for accepting or rejecting the jump proportional to the ratio $k_{Ai}/k_A^{\mathrm{STST}}$. The time taken to complete a jump Ai is the inverse of the total escape rate k_A^{STST} computed either from Eq. (1) or Eq. (3). The details of the validity of the LG simulations with realistic jump frequencies have been explained by Voter.[18] Thousands of randomly generated hops are made and the mean square displacement of the adatom, $\langle \Delta r^2(t) \rangle$, is evaluated as a function of the time, t. The slope of the long time portion of this curve yields the macroscopic diffusion coefficient. These calculations are repeated at a number of different temperatures.

III. COMPUTATIONS AND RESULTS

The simulation system for calculating the energies and frequencies consists of a five layer thick Si slab with eight atoms per layer. The bottom layer is held fixed and the remaining atoms and the Si adatom are allowed to move in the MD simulations. We have chosen to use the Tersoff interaction potential[21] for the Si energetics to be consistent with our previous MD simulations on the adsorption process and the dimer opening mechanisms.[5,8] Following the procedure outlined above we calculated the energy profile of a single adatom on the surface. The energies are reported relative to the fully relaxed adsorbate free Si{100}(2×1) surface. Six local minima are observed and their energetics and geometries are given in Table I. In addition, the energy and dimer length profiles as a function of the surface position are shown in Figs. 1(b) and 1(c). The convergence of the results were checked at all the binding sites with respect to the variations in MD times for the incoming adatom (1–3 ps) and the initial temperature of the substrate (300–1000 K). The results reported here remain converged to within 1%. The values at the energy minima were also checked with a crystal of 18 atoms/layer and were found to be converged to within 5% with no alterations in the qualitative features in the contour plots.

The six local minima are identified by a letter and the number of nearest neighbor atoms of the adatom in the (surface, second, third) layers of the substrate. The long bridge $B(2,4,2)$ and the dimer bridge $D(2,4,2)$ sites are above the fourth layer Si atoms. The cave $C(4,2,2)$ and the hollow $H(4,2,1)$ sites are over the third layer Si atoms. The two other possible binding sites are the on-top sites over the bulk terminated first layer atom, $T(1,2,4)$, and over the second layer atom, $S(2,1,2)$. The T site has also been described as the dangling bond site.

A. Energetics and dynamics of Si adatom adsorption on the clean Si{100}(2×1) surface

The energetic and structural information in Table I and Figs. 1(b) and 1(c) highlight several interesting features of the Si adatom interaction with the Si{100}(2×1) surface. First the global minimum for the surface occurs at site B ($E = -3.43$ eV). However, this site has a very narrow region of the surface over which it occurs and it also corresponds to adsorption close to the surface. Adsorption site T, although higher in energy, has a large region into which incoming atoms can be funneled. [Adsorption site T is the large plateau or mesa region of Fig. 1(b).] These qualitative features of the energy profiles would indicate that adsorption into site T would be more probable than adsorption into site B. We computed these probabilities by simulating MD trajectories of adatom sticking on a clean surface at 0 K and also estimated the relative area of each site on the surface. As seen in Table I, adsorption into sites T, D, and S are most probable. The estimated adsorption probabilities from the relative surface area compare well with those from MD simulations of adsorption trajectories. We also note that the results in Table I are consistent with our previous MD simulations[4,5,8] performed using Tersoff's potential[21] and that of Brenner and Garrison,[22] where the dominant adsorption

TABLE I. Adsorption probabilities, lattice relaxations, and energies of Si adatom on Si{100}-(2×1) surface.

Site	Adsorption probabilities Estimated[a]	Computed[b]	Lattice relaxations Dimer length	d_1[c]	d_2[d]	Coordination	Adatom height[e]	Energy
$B(2,4,2)$	0.08	0.04	2.53 Å	2.43 Å	3.66 Å	2	1.25 Å	−3.43 eV
$D(2,4,2)$	0.18	0.22	3.65 Å	2.30 Å	3.85 Å	2	1.63 Å	−3.26 eV
$S(2,1,2)$	0.16	0.12	2.38 Å	2.45 Å	2.98 Å	≈2	1.69 Å	−2.99 eV
$T(1,2,4)$	0.50	0.63	2.39 Å	2.31 Å	3.93 Å	1	2.31 Å	−2.57 eV
$H(4,2,1)$	0.04	0.00	2.58 Å	2.64 Å	3.26 Å	≈4	1.46 Å	−2.46 eV
$C(4,2,2)$	0.04	0.00	2.35 Å	3.46 Å	2.40 Å	2	0.51 Å	−2.37 eV

[a] Estimated from the relative area of the site on the surface.
[b] Computed from 200 MD trajectories of 6 ps each.
[c] Distance to the nearest surface layer atoms.
[d] Distance to the nearest second layer atoms.
[e] The adatom height is relative to the position of surface atoms in clean relaxed Si{100}-(2×1) surface.

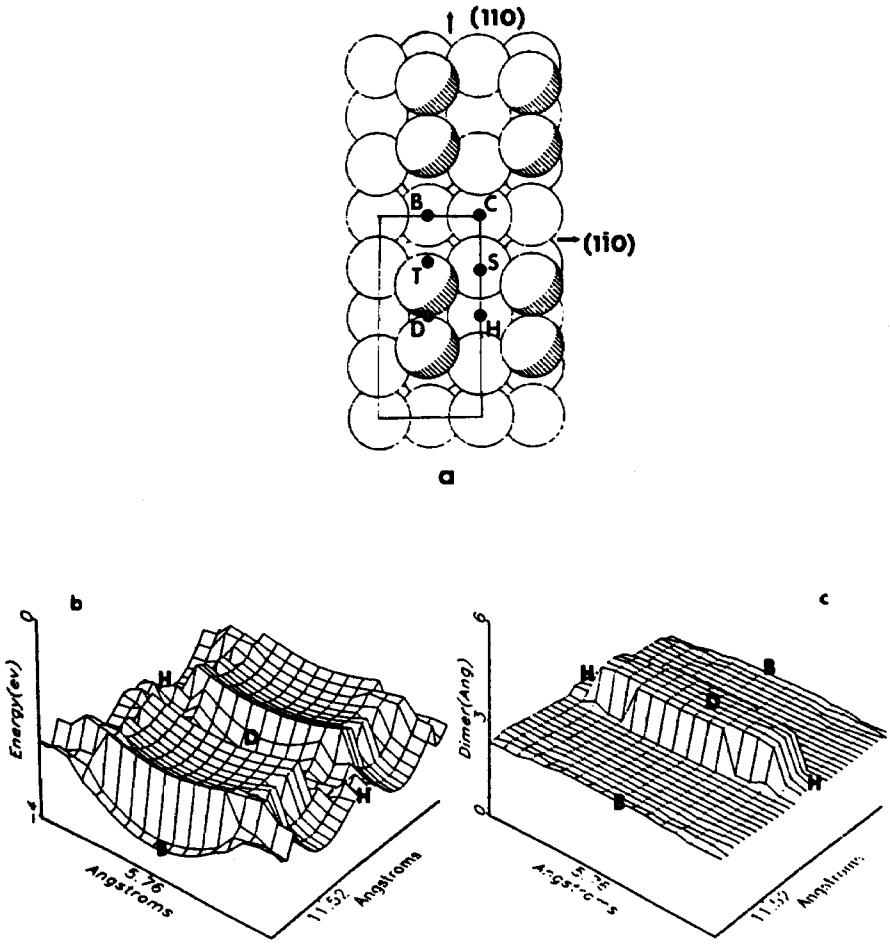

FIG. 1. The Si{100}(2×1) surface. (a) The (2×1) surface unit cell with unique binding sites labeled. The surface dimer atoms are shaded. (b) Energy profile for a single adatom on the surface. (c) Surface dimer bond distance profile.

mechanism was into the dangling bond site.

The dimer length profile in Fig. 1(c) shows quite dramatically that substrate relaxation/rearrangement is critical when considering diffusion of adatoms in a strongly interacting system. For all sites except *D* the surface dimer is closed. However, for the adatom directly above the surface dimer, the dimer spontaneously opens. Adsorption trajectories of this type had been previously observed in MD simulations,[8,23] but, as indicated in Table I, these are not as probable as adsorption into the dangling bond (*T*) site.

Two other energy calculations of profiles, as depicted in Fig. 1(b), have also been reported.[12,13] In one case,[12] the Stillinger–Weber interaction potential[24] was used and seven local minima on the surface were observed. They did not find site *C* to be a minimum and found nearly degenerate pairs of sites near site *B* and site *H*. Their site corresponding to site *B* is lowest in energy and the dangling bond site *T* occupies the largest surface area. They also observe that the dimer is open for site *D*. The other investigation used a modified Tersoff potential with a smoother cutoff function.[13] Again the potential contours are similar although detailed energetics are not presented.

Two *ab initio* local density functional calculations of the energetics of Si adatom adsorption on Si{100}(2×1) have appeared recently.[14,15] In one case[14] the global minimum is at the *H* site and the dimer opens for the adsorption at the *B* and *C* sites. In the other study[15] the dimer remains closed for all the adsorption sites and the global minimum is at the *S* site. We note that in these studies[14,15] pseudopotentials from two different sources have been used.[25,26] The results of these studies are significantly different from each other and also from those in Figs. 1(b) and 1(c) (this work) and the other empirical potential calculations.[12,13] Our results in Figs. 1(b) and 1(c) are in qualitative agreement with the other empirical potential calculations.[12,13] It is interesting that the Stillinger–Weber[24] and Tersoff[21] potentials give similar results, as they were functionalized and fit with very different philosophies. The SW function penalizes geometries that are not tetrahedral and was fit to diamond lattice and liquid type structures. The Tersoff potential has a very different angular dependence and was fit to the energetics and structure of small clusters as well as bulk configurations. The angular dependence is not a penalty for nontetrahedral geometries. At this point, then, the correct surface energetics are not known. We feel that it is useful to pursue the consequences of the Tersoff potential in the STST and LG calculations. Ultimately the final test will be comparison to experiment or a higher level of *ab initio* calculation.

B. Rate constants for elementary diffusion jumps

The contour plot of the surface energetics presents a preview of the nature of the diffusion process but does not

TABLE II. The adatom diffusion dynamics on Si{100}-(2×1) surface at 600 K.

Jump type	Activation[a] energy (eV)	Vibrational[a] frequency (s^{-1})	Total escape[b] rates (s^{-1})	Jump[b] probabilities	Total escape[c] rates	Jump[c] probabilities
$B\rightarrow T$	1.42	0.45×10^{13}	2.39×10^{3}	0.002	9.44×10^{3}	0.001
$B\rightarrow C$	1.08	0.14×10^{13}		0.498		0.499
$D\rightarrow T$	1.08	0.75×10^{13}	8.51×10^{6}	0.001	2.41×10^{7}	0.001
$D\rightarrow H$	0.71	0.39×10^{13}		0.499		0.499
$S\rightarrow C$	0.79	0.66×10^{13}		0.007		0.005
$S\rightarrow T$	0.96	0.95×10^{13}	2.33×10^{8}	0.000	6.46×10^{8}	0.001
$S\rightarrow H$	0.52	0.54×10^{13}		0.993		0.993
$H\rightarrow S$	0.10	0.56×10^{13}	6.31×10^{12}	0.128	1.42×10^{13}	0.143
$H\rightarrow D$	0.03	0.42×10^{13}		0.372		0.357
$T\rightarrow S$	0.43	0.15×10^{13}		0.032		0.030
$T\rightarrow D$	0.28	0.23×10^{13}	1.14×10^{10}	0.895	4.44×10^{10}	0.914
$T\rightarrow B$	0.45	0.28×10^{13}		0.041		0.026
$C\rightarrow B$	0.03	0.16×10^{13}	2.19×10^{12}	0.409	1.13×10^{13}	0.435
$C\rightarrow S$	0.18	0.64×10^{13}		0.091		0.065

[a] Computed on the 0 K potential surface of Fig. 1(b).
[b] Computed from Eqs. (1) and (2).
[c] Computed from Eqs. (3)–(8).

definitively describe the diffusion rates. To determine these we have also calculated the activation barriers between each of the sites. From Fig. 1(b), we note that the minimum activation barriers from all the labeled sites are generally along the two orthogonal directions thus using a sum over only four directions in Eq. (3a) is justified. The activation barriers and jump frequencies, therefore, as calculated by Eq. (2), are given in Table II. The activation barriers vary from 0.03 eV ($C\rightarrow B$) to 1.42 eV ($B\rightarrow T$). These are large differences given that this energy is used in the Boltzmann factor. The vibrational frequencies, on the other hand, are used as prefactors and thus the values of $0.14\text{–}0.95\times10^{13}$ s^{-1} are nearly constant. Using the activation energies and vibrational frequencies in Eq. (1) the total escape rates, k_A^{STST}, can be calculated. These values for a temperature of 600K are given in Table II.

The escape rates from the various sites, as given in Table II, vary from 10^3 to 10^{12} per second. Correspondingly, the residence times vary from milliseconds to picoseconds. Naturally the longest residence time is for site B, the most stable site. However, even in this site the adatom has sufficient time to diffuse during MBE growth that is occurring at the rate of 0.1 to 1 layer per minute.[1] In addition to the overall escape rates, Table II also has the individual jump probabilities. For example, the total escape rate from site T is 1.14×10^{10} s^{-1}. Of the total hops, 90% of the time the adatom moves into site D, 4% into site B, and 3% each into the two equivalent adjacent S sites. Since the adsorption of the adatom occurs primarily in sites T, D, and S (Table I), the most important jumps are $T\rightarrow D$, $S\rightarrow H$, and $D\leftrightarrow H$. The first two jumps center the randomly deposited adatom onto the nearest dimer row and the last two, $D\leftrightarrow H$, provide a path for the diffusion of the adatom along the dimer row. Also given in Table II are the temperature corrected values for the escape rates and jump probabilities, Eqs. (3)–(8). The values of the rates increase by factors of 2–4 but the ordering of the relative rates does not change.

C. Lattice gas simulations for the diffusion

The relative escape rates and jump frequencies from the various sites are useful for estimating the dominant path of diffusion, but, as mentioned above, diffusion out of even the B site can occur during the MBE growth event. Lattice gas simulations allow one to obtain a better idea of the actual diffusive processes. Correspondingly, LG simulations were performed at temperatures of 300, 600, 800, and 1000 K for both the escape rates, as calculated by Eq. (1), and for the temperature corrected values, as determined by Eq. (3). In Fig. 2 two sample "trajectories" of migration are shown. Each dot represents a hop into that particular site. In approximately 95% of the "trajectories" that lasted up to 50 μs, the adatom followed a path similar to that shown in trajectory 1. For the most part the adatom remains on the dimer

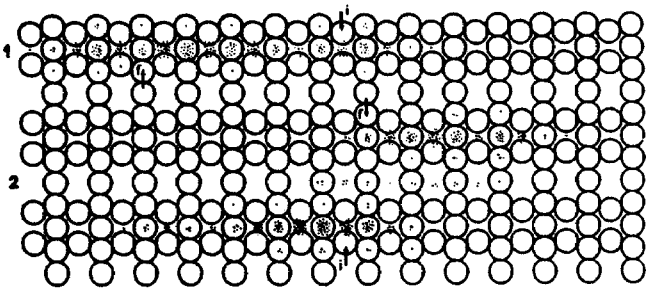

FIG. 2. Two sample trajectories of macroscopic migration. The arrows indicate the initial and the final positions of the migrating adatom and each dot in a trajectory represents a hop into that particular site. The labels i and f indicate the initial and final positions.

row, migrating between H and D sites. Occasionally there are side excursions to a T site. The microscopic mechanism of this dominant diffusion path from $H \leftrightarrow D$ is depicted in Fig. 3. In Fig. 3(a) the adatom is in site D and the dimer at position 1 is open. A $D \rightarrow H$ jump [Fig. 3(b)] involves a spontaneous closing of the dimer at position 1. Finally an H to D jump will open the dimer at position 2. Of note is that the dominant mechanism of adatom diffusion is intimately intertwined with the surface reconstruction. The dimers are opening and closing as the adatom diffuses. The second trajectory depicted in Fig. 2 shows that the adatom can occasionally diffuse into the trough between two dimer rows, diffuse among B and C sites, and then eventually make it to the adjacent dimer row. Although this type of motion is not as probable as diffusion along only one dimer row, it can easily occur on the time scale of the MBE growth. Of note is that the LG calculations demonstrate quite clearly that the diffusion is anisotropic and is parallel to the dimer rows. The main mechanism of diffusion involves hopping between H and D sites, although hopping between B and C sites in the trough yields the same anisotropy.

The LG calculations, in addition to the mechanism of diffusion, yield the macroscopic diffusion constant. The diffusion coefficients at four temperatures, both with and without the thermal vibration corrections, are plotted in Arrhenius form in Fig. 4. A best fit to the two sets of data yields that the Arrhenius behavior for the self-diffusion of Si on Si{100}(2×1) follows $D = 7.2 \times 10^{-4} \exp(-0.72\ \text{eV}/kT)$ cm^2/s with no thermal vibrational correction and $D = 5.7 \times 10^{-3} \exp(-0.75\ \text{eV}/kT)$ cm^2/s with the thermal vibrational corrections. Of note is that even though the thermal corrections change the values in the diffusion coefficient, the microscopic mechanism of diffusion is in no way altered.

D. Comparison with experimental results

The rate of self-diffusion of Si on Si substrates has been a desired quantity for estimating growth conditions in MBE for many years. However, it has only been with the advent of scanning tunneling microscopy (STM) that reliable experimental quantities have become available. For comparison to our calculations we are interested in the activation energy of diffusion, the overall diffusion coefficient, and any possible directionality or anisotropy.

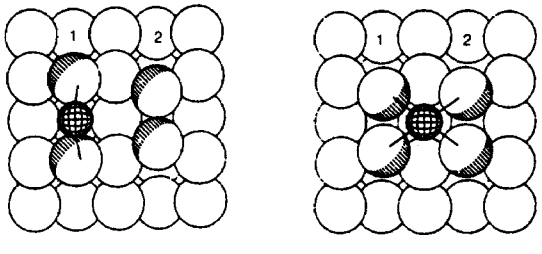

FIG. 3. Reconstruction aided diffusion mechanism. (a) Adatom (hatched) in site D. (b) Adatom in site H.

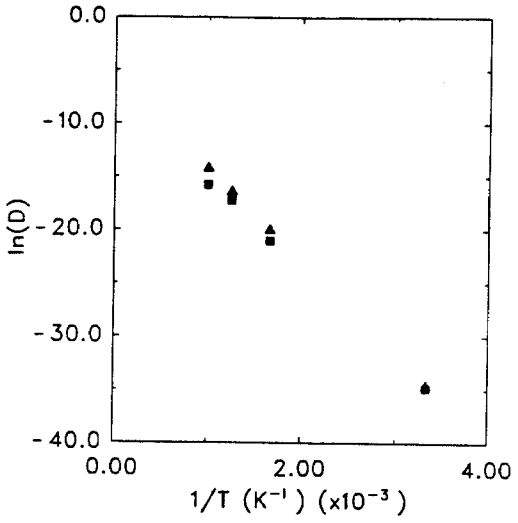

FIG. 4. Logarithm of the diffusion coefficient as a function of inverse temperature. The squares correspond to the lattice gas simulations using the energy profile in Fig. 1(b). The triangles represent the calculation where the thermal vibrational corrections have been included.

Initial experimental estimates of the activation energy for Si self-diffusion indicated that the value was less than 1.1 eV.[27-29] In the most recent study of Si self-diffusion on Si{100}(2×1) by STM, Lagally and co-workers[19,20] have found the activation energy to be 0.67 ± 0.08 eV and the prefactor to be $\sim 10^{-3}$ cm^2/s.[20] Our corresponding values of 0.75 eV and 5.7×10^{-3} cm^2/s are within their experimental error bars, especially given that there are statistical uncertainties associated with the LG simulations and also the empirical potential. Of note is that the macroscopic activation energy cannot simply be obtained from the energy profile of Fig. 1(b). It is a convoluted average of many of the individual activation energies, although it is quite close to the value for the rate limiting step ($D \rightarrow H$) along the main diffusion path. Moreover, the STM studies clearly demonstrate that the direction of diffusion is strongly anisotropic and parallel to the dimer rows. As the other calculations of the energy profiles[12,13] did not include a lattice gas simulation, it is difficult to make direct comparisons of the activation energies.

It is important to bear in mind that these (and other) calculations to date have been for a single adatom on a perfect surface. The experiments are performed on surfaces with steps, islands, and defects. For diffusion near such features similar calculations must be performed (and, in fact, are underway). In addition, there is a basic assumption that the adatom remains the adatom. In a previous simulation of the growth process, mechanisms where the adatom exchanged with a surface atom were observed.[8,23] Again, this assumption can be removed, but a separate calculation must be performed.

IV. SUMMARY

Lattice gas simulations of a Si adatom self-diffusion on the fully relaxed Si{100}(2×1) surface have been per-

formed. The site to site jump frequencies for all possible elementary diffusion hops between many local binding sites were obtained from a combination of molecular dynamics simulations and simplified transition state theory. We find that there are six unique local binding sites on the surface. The global minimum is the bridge site, B, in the trough between two dimers. However, the most probable adsorption site of a Si atom from the gas phase is into the dangling bond or T site.

The macroscopic diffusion process is calculated to follow the Arrhenius form, $D = 5.7 \times 10^{-3} \exp(-0.75\ \text{eV}/kT)\ \text{cm}^2/\text{s}$. Our values of the activation energy and prefactor agree well with the experimental values of 0.67 ± 0.08 eV and $\sim 10^{-3}\ \text{cm}^2/\text{s}$. Moreover, both our calculations and the experiments show that the diffusion is highly anisotropic with the direction of motion being parallel to the dimer rows. Our mechanism of diffusion indicates that the surface dimers open and close as the adatom migrates along the top of the dimer row.

ACKNOWLEDGMENTS

We gratefully thank the Office of Naval Research, the National Science Foundation, the IBM Program for the Support of Materials and Processing Sciences, and the Camille and Henry Dreyfus Foundation for financial support. The Pennsylvania State University supplied a generous grant of computer time for this work.

[1] H. J. Gossmann and L. C. Feldman, Phys. Rev. B **32**, 6 (1985).
[2] T. Sakamoto, N. J. Kawai, T. Nakagawa, K. Ohta, and T. Kojima, Appl. Phys. Lett. **47**, 617 (1985).
[3] R. M. Tromp, R. J. Hamers, and J. E. Demuth, Phys. Rev. Lett. **55**, 1303 (1985).
[4] D. W. Brenner and B. J. Garrison, Surf. Sci. **198**, 151 (1988).
[5] D. Srivastava, B. J. Garrison, and D. W. Brenner, Phys. Rev. Lett. **63**, 302 (1989).
[6] M. R. Wilby, S. Clarke, T. Kawamura, and D. D. Vvedensky, Phys. Rev. B **40**, 10617 (1989).
[7] J. Y. Tsao, E. Chason, U. Köhler, and R. Hamers, Phys. Rev. B **40**, 11951 (1989).
[8] D. Srivastava, B. J. Garrison, and D. W. Brenner, Langmuir **7**, 683 (1991).
[9] R. J. Hamers, U. K. Köhler, and J. E. Demuth, Ultramicroscopy **31**, 10 (1989).
[10] M. G. Lagally, R. Kariotis, B. S. Swartzentruber, and Y. W. Mo, Ultramicroscopy **31**, 87 (1989).
[11] A. J. Hoeven, J. M. Lenssinck, D. Dijkkamp, E. J. Van Loenen, and J. Dieleman, Phys. Rev. Lett. **63**, 1830 (1989).
[12] Z. Zhang, Y. Lu, and H. Metiu, Surf. Sci. **248**, L250 (1991).
[13] J. Wang and A. Rockett, Phys. Rev. B **43**, 12571 (1991).
[14] T. Miyazaki, H. Hiramoto, and M. Okazaki, Jpn. J. Appl. Phys. **29**, L1165 (1990).
[15] G. Brocks, P. J. Kelly, and R. Car, Phys. Rev. Lett. **66**, 1729 (1991).
[16] For a recent review see, for example, D. G. Truhlar, A. D. Isaacson, and B. C. Garrett, *Theory of Chemical Reaction Dynamics Vol. IV*, edited by M. Bayer (CRC, Boca Raton, FL, 1985) and references therein.
[17] A. F. Voter and J. D. Doll, J. Chem. Phys. **82**, 80 (1985).
[18] A. F. Voter, Phys. Rev. B **34**, 6819 (1986).
[19] Y. W. Mo, R. Kariotis, B. S. Swartzentruber, M. B. Webb, and M. G. Lagally, J. Vac. Sci. Technol. A **8**, 201 (1990).
[20] Y. W. Mo, J. Kleiner, M. B. Webb, and M. G. Lagally, Phys. Rev. Lett. **66**, 1998 (1991).
[21] J. Tersoff, Phys. Rev. B **39**, 5566 (1989).
[22] D. W. Brenner and B. J. Garrison, Phys. Rev. B **34**, 1304 (1986).
[23] D. Srivastava and B. J. Garrison, J. Vac. Sci. Technol. A **8**, 3506 (1990).
[24] F. Stillinger and T. Weber, Phys. Rev. B **31**, 5262 (1985).
[25] J. Ihm and M. L. Cohen, Solid State Commun. **29**, 711 (1979).
[26] G. B. Bachelet, D. R. Hamann, and M. Schlüter, Phys. Rev. B **26**, 4199 (1982).
[27] E. Kasper, Appl. Phys. A **28**, 129 (1982).
[28] M. Ishikawa and T. Doi, Appl. Phys. Lett. **50**, 1141 (1987).
[29] T. Sakamoto, N. J. Kawai, T. Nakagawa, K. Ohta, and T. Koima, Appl. Phys. Lett. **47**, 617 (1985).